Eur. Phys. J. B **70**, 443–447 (2009)
DOI: 10.1140/epjb/e2009-00242-0

THE EUROPEAN PHYSICAL JOURNAL B

Regular Article

Far IR spectra of Ag_2CdI_4 at temperature range 10–420 K: complementary experimental and first-principle theoretical study

I. Karbovnyk[1], S. Piskunov[2,3,a], I. Bolesta[1], S. Bellucci[4], M. Cestelli Guidi[4], M. Piccinini[4], E. Spohr[2], and A.I. Popov[3,5]

[1] Department of Electronics, Ivan Franko National University of Lviv, 107 Tarnavskogo street, 79017 Lviv, Ukraine
[2] Lehrstuhl für theoretische Chemie, Universität Duisburg-Essen, Universitätstr. 2, 45141 Essen, Germany
[3] Institute of Solid State Physics, University of Latvia, 8 Kengaraga Street, 1063 Riga, Latvia
[4] INFN-Laboratori Nazionali di Frascati, via E. Fermi 40, 00044 Frascati, Italy
[5] Institut Laue-Langevin, 6 rue Jules Horowitz, 38042 Grenoble, France

Received 9 October 2008 / Received in final form 6 May 2009
Published online 15 July 2009 –

Abstract. The influence of temperature on the far-infrared (FIR) spectrum of polycrystalline Ag_2CdI_4 has been investigated by Fourier Transform Infrared (FTIR) spectroscopy measurements. The FIR phonon spectrum has also been calculated by means of quantum mechanical density functional theory (DFT). The comparison of calculated and measured spectra allows the fast and reliable assignment of the measured phonon modes, and thus clarifies the mode splitting character obtained at elevated temperatures.

PACS. 71.15.Mb Density functional theory, local density approximation, gradient and other corrections – 78.30.Hv Other nonmetallic inorganics

1 Introduction

Ag_2MX_4 compounds, where M = Cd, Hg, Zn, etc., belong to a class of *superionic solids* which are promising materials for use in solid state batteries and fuel cells due to extraordinarily high ionic conductivity at supercritical temperatures [1]. In such ternary superionic conductors mobile ions of different type contribute to the total electric conductivity and thus result in different vibration frequencies. In their turn, the vibration frequencies reflect the interaction between the lattice and charge carriers. From this point of view IR spectroscopy provides an effective understanding of resonant processes in solid electrolytes as it is very sensitive to temperature induced phase transitions affecting nearest neighbor dynamics. Although the lattice dynamics of Ag_2MX_4 family representatives was extensively studied (see Refs. [2,3] and references therein), results obtained for Ag_2CdI_4 are extremely scarce in the literature. Only one study reporting Raman and infrared (IR) spectroscopy of low frequency dynamics in Ag_2CdI_4 at 300 K appeared so far [4]. However, due to the significant broadening of the infrared reflectivity spectrum at 300 K, it is not possible to resolve clearly and characterize the phonon modes associated with the stretching vibrations of Ag-I bonds and with the bending modes of the Cd-I complex. Therefore Ag_2CdI_4 remains the only compound in the Ag_2MX_4 family for which complete information describing the material properties in the FIR domain is effectively missing. Motivated by this situation, in the present study we complement the detailed experimental FTIR measurements with the phonon spectra calculated from quantum mechanical density functional theory. Such an approach is an effective method for the phonon mode identification in relatively complex systems (see e.g. Ref. [5]). In our study we make use of the fact that the important dielectric parameters can be derived from factorized fitting and Kramers-Kronig analysis, but since superionic conductivity is straightly related to phonon density of states an important complementary information can be extracted from first-principle calculations. Thus, this respect to mentioned above, Ag2CdI4 as a ternary derivative of the "classic" solid electrolyte, AgI, is an interesting model material to study by combining theoretical and experimental techniques from methodological considerations as well.

2 Experimental procedure

In the AgI-CdI_2 system, Ag_2CdI_4 is the only chemical compound stable at ambient conditions [6]. Bulk polycrystalline samples of Ag_2CdI_4 were obtained by solid state chemical reactions as described elsewhere [7–9]. Approximately 5 mm thick cylindrical pellets with diameter of about 10 mm were prepared. Pellet surfaces were carefully polished in several stages in order to ensure maximum intensity of the reflected signal. IR spectroscopy was performed at the Daphne Light synchrotron IR facility, which is described in [10] and intensively used for nondestructive

[a] e-mail: piskunov@lu.lv

quantitative characterization of different types of the micro- and nanomaterials [11–15]. A BRUKER Equinox 55 interferometer modified to work under vacuum and a Helitran LT-3 cryostat were employed to collect FIR spectra in the temperature range of 10–420 K. Measurements were performed for non-polarized light with a resolution of 1 cm^{-1} in the frequency range from 35 to 600 cm^{-1}. The reflected signal was detected using a Si bolometer, cooled to 4.2 K, which is capable of working in the energy range 10–700 cm^{-1}. Preliminary experimental data processing and Kramers-Kronig analysis were performed using Bruker's OPUS spectroscopic software. For spectra fitting purposes we used the FOCUS optical functions creation utility.

3 Computational details

Quantum-mechanical total energy calculations of ε-Ag_2CdI_4 in its low-temperature tetragonal phase ($I\bar{4}2m$) were carried out with the latest version of the CRYSTAL06 computer code [16], which employs Gaussian-type functions centered on atomic nuclei as basis set (BS) for expansion of the crystalline orbitals. The Hay-Wadt small-core effective pseudopotential was used to represent inner electrons of Ag, while the outer electron shells were described by a BS in the form of 311d31G [16]. An all-electron BS in the form of 9-76(d6)311d31G was used for Cd, and iodine atoms are described by a Hay-Wadt large-core pseudopotential and the BS in the form of 31G [16]. In order to provide balanced summation in direct and reciprocal lattices the reciprocal space integration was performed by sampling the Brillouin zone with the $8 \times 8 \times 8$ Pack-Monkhorst mesh [17], which for tetragonal Ag_2CdI_4 results in 59 k-points in total. The cutoff threshold parameters of CRYSTAL for Coulomb and exchange integrals evaluation (ITOL1-ITOL5) have been set to 8, 8, 8, 8, and 16, respectively. Calculations were considered as converged only when the total energy differs by less than 10^{-9} a.u. in two successive cycles of the self-consistency procedure. The central-zone vibrational spectrum of ε-Ag_2CdI_4 is calculated by building the Hessian matrix numerically from the analytical gradients of the energy with respect to the atomic coordinates. The mass-weighted hessian matrix is diagonalized to obtain eigenvalues, which are converted to frequencies, and eigenvectors, which are the normal modes. Normal modes reported in terms of the atomic cartesian displacements normalized to classical amplitudes allow us to perform the precise assignment of vibrational modes. The nonanalytical part is obtained with a finite field supercell approach for the high-frequency dielectric constant and a Wannier function scheme for the evaluation of Born charges (for details see [16] and references therein). The dielectric tensor components, ε_{xx} and ε_{zz}, are evaluated at $N = 6$ (size of supercell).

4 Results and discussion

Figure 1 shows the experimental temperature dependence of the FIR reflectivity of Ag_2CdI_4. At the lowest measured

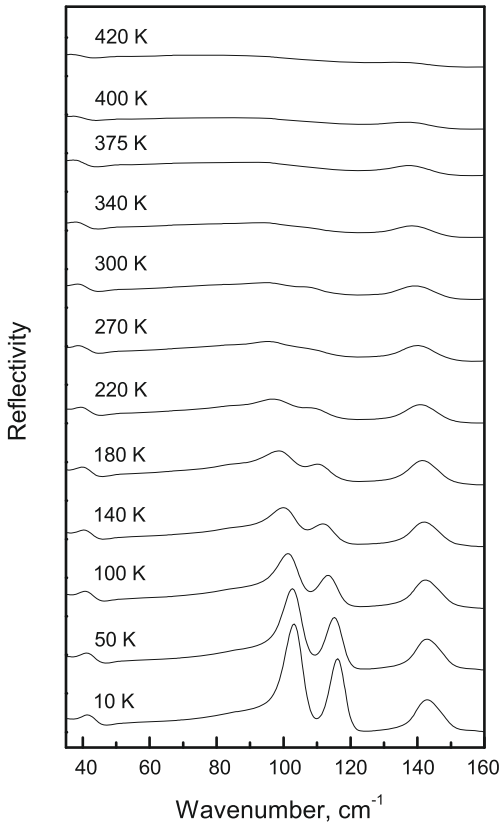

Fig. 1. Temperature evolution of FIR reflectivity of Ag_2CdI_4.

temperature one can unambiguously address four sharp features in the range 35–160 cm^{-1} which are directly related to IR active processes. To obtain the parameters which describe the observed phonon modes we exploit the factorized Lyddane-Sachs-Teller equation which incorporates the transverse and longitudinal frequencies ($\omega_{i\mathrm{TO}}$ and $\omega_{i\mathrm{LO}}$) and the respective damping factors ($\Gamma_{i\mathrm{TO}}$ and $\Gamma_{i\mathrm{LO}}$) for each mode i [18,19]:

$$\varepsilon(\omega) = \varepsilon_\infty \prod_i \frac{\omega_{i\mathrm{LO}}^2 - \omega^2 + j\Gamma_{i\mathrm{LO}}\omega}{\omega_{i\mathrm{TO}}^2 - \omega^2 + j\Gamma_{i\mathrm{TO}}\omega}, \tag{1}$$

where ε_∞ stands for the high frequency dielectric constant and $j^2 = -1$. Equation (1) can describe the significant LO-TO splitting for ionic crystals in good approximation [20]. Combined with the known Fresnel relation between the reflectivity factor R and the dielectric function ε [21,22], which for the case of near normal incidence simplifies to the form

$$R = \left| \frac{\varepsilon^{\frac{1}{2}} - 1}{\varepsilon^{\frac{1}{2}} + 1} \right|^2, \tag{2}$$

allows for constructing the model spectrum $R(\omega)$. Equations (1) and (2) have been successfully applied in the investigations of various solid-state systems, including superionic conductors [23]. We have performed a non-linear least squares fit to adjust the parameters of equation (1)

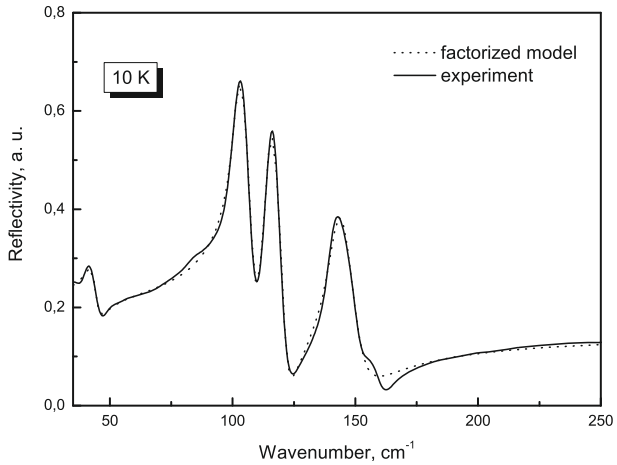

Fig. 2. Frequency dependence of FIR reflectivity of Ag_2CdI_4 at 10 K. Solid line corresponds to the experimental spectrum. Dotted line represents the reflectivity factor calculated from Fresnel's formula assuming the dielectric function in equation (1).

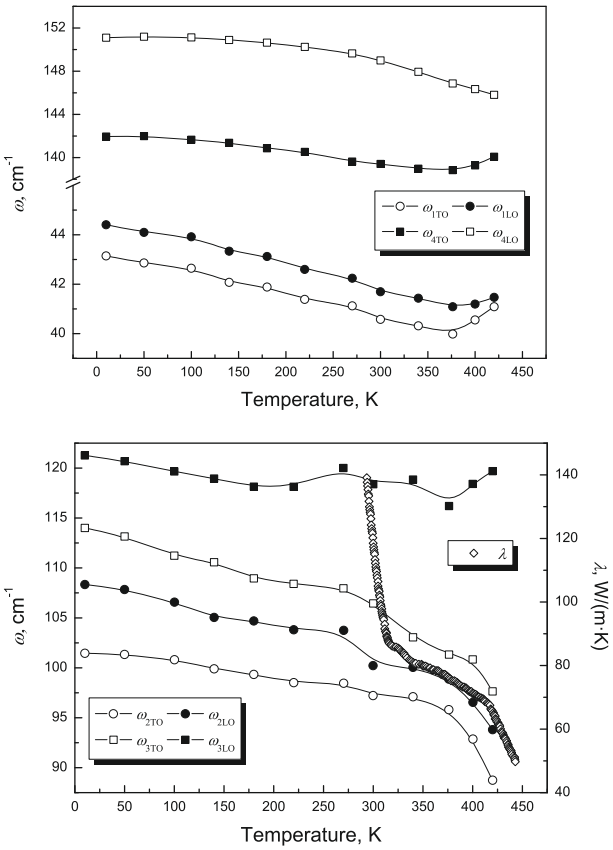

Fig. 3. Temperature dependences of LO and TO phonon frequencies in Ag_2CdI_4, as derived by non-linear least squares fitting of the experimental reflectivity assuming the dielectric constant to be in the form of equation (1). The thermal conductivity λ of Ag_2CdI_4 (diamonds) [7] is plotted together with the phonon frequencies in the lower part of the figure. Solid lines are to guide the eye.

for each studied temperature. The result of this modeling at $T = 10$ K is shown in Figure 2. ε_∞ was found to decrease from 3.43 at 10 K to 3.15 at 420 K. Total mean square deviation between the curves in Figure 2 is less than 0.035 and the fitting accuracy increases as one goes to higher temperatures. The LO and TO frequencies, determined by fitting the experimental reflectivity with Fresnel's formula and taking into account equation (1), have been plotted in Figure 3 versus temperature. The frequency of the ω_1 mode decreases slightly upon heating to approximately 375 K, with nearly constant LO-TO splitting below this temperature. Similar behavior is observed in the case of the ω_4 mode. For both modes there is a "switching point" between 370 and 380 K where the respective frequencies begin to increase and the LO-TO splitting begins to decrease. The two other optical phonon modes exhibit more complicated temperature behavior. ω_{3LO} shows generally a smooth decrease versus temperature below 250 K, fluctuations around 119 cm^{-1} between 250 and 350 K and a linear increase starting from 375 K. Some deviations in $\omega_{3LO}(T)$ at higher temperatures which might be due to the significant overlapping of ω_2 and ω_3 bands above room temperature and/or some uncertainty in the determination of the exact phonon frequency. It is also obvious from the lower part of Figure 3 that there is a correlation between the $\omega_{2TO}(T)$, $\omega_{3TO}(T)$, and $\omega_{2LO}(T)$ curves and the thermal conductivity $\lambda(T)$ (data taken from [7]). Thus, one obviously can not neglect the contribution of optical phonons to the thermal conductivity of Ag_2CdI_4. Although it is expected that melting of the silver sublattice should lead to abrupt changes in the temperature dependencies of phonon modes ascribed to Ag-I vibrations, this kind of behavior is not observed in Figure 3. One possible explanation is the blurring of the phase transition in Ag_2CdI_4, in the sense that the compound transforms into the superionic state through a series of intermediate mixed phases [1,6]. According to [2], ternary compounds derived from silver iodide remain indeed ordered even very close to (but still below) the superionic transition temperature. In our case, the transition temperature might be yet out of the range of measurements, therefore we do not observe abrupt changes in Figure 3.

Although our IR spectrum partly correlates with the one published in reference [4], the mode splitting character in our case is completely different. In reference [4] LO and TO modes are identified as minimum and maximum points in the room temperature reflection spectrum, respectively. One should notice, however, that such identification may contain substantial error, whereas the reflection spectrum at 300 K (as it is clear from Fig. 1 and as well from the corresponding spectrum in Ref. [4]) does not allow for the precise determination of minimum and maximum points. Here we used a more accurate procedure. Furthermore, in addition to the dielectric response modeling within the factorized approach, we have extracted LO and TO frequencies from the Im $\varepsilon(\omega)$ and Re $\varepsilon(\omega)$ curves calculated on the basis of the Kramers-Kronig analysis of the experimentally measured spectra. We should note here, that due to the fact that the wavelengths of FIR

Table 1. Lattice constants a_0 and c_0 (in Å), atomic coordinates $I(x)$ and $I(z)$ (in fractional units), components of dielectric tensor (ε_{xx} and ε_{zz}, can be compared to the isotropic dielectric constant of 3.43 obtained from the measurements at 10 K), and frequencies of IR-active TO and LO modes (in cm^{-1}) of ε-Ag_2CdI_4 as calculated by means of GGA and hybrid exchange-correlation functionals within DFT. Calculated intensities of IR modes are given in brackets (in KM/mol). Two numbers in a row correspond to TO/LO frequencies.

	PW	PBE	B3PW	B3LYP	Exp.
a_0	6.4935	6.5070	6.5102	6.7240	6.3338[1]
c_0	13.2472	13.3039	13.2738	13.4492	12.6807[1]
$I(x)$	0.2661	0.2631	0.2655	0.2655	0.2667[1]
$I(z)$	0.1153	0.1156	0.1154	0.1181	0.1183[1]
ε_{xx}	2.668	2.643	2.434	2.326	
ε_{zz}	2.736	2.710	2.494	2.372	
E	31(3)/32(1)	30(3)/31(1)	31(3)/32(1)	29(4)/30(1)	
E	38(0)/38(0)	38(0)/38(0)	40(0)/40(0)	41(0)/41(0)	
B_2	49(8)/52(2)	49(8)/52(2)	50(9)/53(2)	50(1)/51(1)	43/44[2]
E	99(59)/99(0)	97(91)/111(51)	99(0)/99(0)	91(49)/92(2)	
E	100(69)/113(53)	98(38)/98(0)	99(121)/113(48)	94(78)/108(50)	101/108[2]
B_2	101(68)/112(16)	99(70)/111(16)	101(65)/113(16)	92(1)/92(0)	
B_2	132(65)/155(122)	130(63)/153(123)	134(62)/158(118)	133(19)/133(5)	114/121[2]
E	143(108)/160(186)	140(108)/158(188)	144(108)/162(184)	139(110)/158(190)	141/151[2]

[1] Taken from powder diffraction study [6]. [2] Measured in present study at 10 K.

emission are comparable to the average grain size in the samples of polycrystalline Ag_2CdI_4, the effective medium approximation (EMA) approach cannot be properly applied for the evaluation of measured phonon spectra [24].

In this study, we report results of quantum chemical calculations performed using four different generalized gradient approximation (GGA) exchange-correlation functionals within DFT. Table 1 shows equilibrium geometries, dielectric tensor components, and frequencies and intensities of visible IR-active TO-LO phonon modes as calculated using the Perdew-Wang (PW) [25,26], the Perdew-Burke-Ernzerhof (PBE) [27], and the two three-parameter "hybrid" GGA functionals B3PW and B3LYP [28] (which involve admixtures of non-local Fock exact exchange). The internal coordinates and cell parameters of ε-Ag_2CdI_4 have been fully optimized for each Hamiltonian considered. Here we note that B3LYP was less adequate to describe both bulk and vibrational properties of Ag_2CdI_4, while results obtained using other GGA functionals correlate well with each other and are in relatively good agreement with experimental observation (see Tab. 1). In this study we do not consider the local density approximation and Hartree-Fock Hamiltonians which are known to be unprecise in estimation of vibrational properties of wide-gap materials [29]. In further discussion we refer to calculations performed with the PW Hamiltonian.

The theoretical factor group analysis indicates that the phonon modes of tetragonal ε-Ag_2CdI_4 ($I\bar{4}2m$) at the Γ point can be decomposed as [30]:

$$\Gamma = 2A_1(\mathrm{R}) + A_2 + 2B_1(\mathrm{R}) + 4B_2(\mathrm{IR,R}) + 6E(\mathrm{IR,R}). \quad (3)$$

In total there are 8 modes of B_2 and E symmetry being IR active, and two acoustic modes (B_2 and E) yield zero frequencies at the Γ point. Since the sample under study has a polycrystalline structure, on the one hand the mode symmetry cannot be directly assigned on the basis of the measured FIR response, on the other hand analysis of vibrational modes (intensities) calculated from first principles is a fast (calculations just take a few hours on a dual-socket quad-core machine) and reliable tool to validate the measured low temperature FIR spectra. Observable optical IR-active LO-TO phonon modes are also listed in Table 1. In Figure 4 we have plotted the IR-active TO phonon mode intensities for the PW Hamiltonian, as well as those measured experimentally at 10 K. For the purpose of comparison, calculated intensities were used to create a model spectrum by means of a Gaussian fit. Each calculated intensity was fitted with a sum of four Gaussians ($FWHM = 19$). FIR measurements at 10 K yield four well-recognizable peaks at 43, 101, 114, and 141 cm^{-1} which correspond to four calculated peaks at 49, 100, 132, and 143 cm^{-1}. The calculated shifts between TO and LO optical modes are in good agreement with those derived from experiment (Tab. 1). IR modes of E symmetry near the low-energy limit of the range of measurements ($\sim$31 and $\sim$38 cm^{-1}) have very low intensities of 3.08 and 0.02 KM/mol, respectively and thus are neither observed experimentally nor distinct in the calculated spectrum. The weak shoulder at $\sim$155 cm^{-1} is recognizable only in the spectrum at 10 K. It is invisible at elevated temperatures. Also, it does not appear in the calculated spectrum. A reliable assignment for the 155 cm^{-1} peak at 10 K can be made only with a higher resolution IR spectroscopic study (using an upgraded instrument).

In agreement with measured spectra, our calculations exhibit four IR-frequency bands. Three of four calculated bands are in line with the experiment, while the bands around 132 cm^{-1} (calculations) and around 114 cm^{-1}

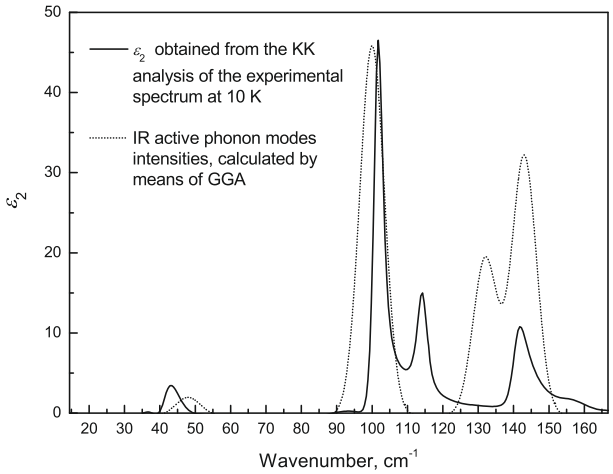

Fig. 4. Calculated phonon modes intensities as compared to the peaks of the imaginary part of the dielectric function.

(measurements) cannot be brought into correlation easily. In an attempt to resolve this issue we arrived at the conclusion that the used BS for iodine is rather incomplete, which also leads to a discrepancy of the calculated lattice constant c_0 of tetragonal ε-Ag_2CdI_4, the narrower calculated peak around 100 cm^{-1}, and the additional split of the peak in the vicinity of 140 cm^{-1}. This points towards the necessity of optimization of the iodine BS, that is, however, beyond the scope of the current study. The B_2 mode around 49 cm^{-1} (43 cm^{-1} in experiment) is assigned to be a weak rotation of a Cd-I complex. The measured peak around 101 cm^{-1} consists of two E and one B_2 modes, which are stretching and bending modes of Ag-I, respectively. The B_2 mode around 132 cm^{-1} (114 cm^{-1} in experiment) and E mode around 143 cm^{-1} are Cd-I stretching modes.

5 Conclusions

In summary, we have performed a complete IR characterization of the ternary superionic compound Ag_2CdI_4. We complement FTIR spectroscopy with Kramers-Kronig analysis and complex dielectric response modeling with a number of quantum-chemical DFT calculations of the central-zone vibrational spectrum of Ag_2CdI_4. This combination of different techniques allowed us to validate the IR-active optical modes, describe mode splitting in polycrystalline Ag_2CdI_4, obtain dielectric parameters in the IR-range and thus bridge the gap in studying of Ag_2MX_4 superionic compounds. The present approach can be further applied to study the lattice dynamics in other complex polycrystalline solids.

The authors are grateful for many fruitful discussions with Dr. Yu. Zhukovskii. This work was supported by the European Commission through the TARI project No. 55 and by the Latvian LZP grant Nr. 09.1127. Ivan Karbovnyk greatly appreciates the support from INTAS in the frame of Young Scientist Fellowship Nr. 06-1000019-6325.

References

1. S. Hull, Rep. Prog. Phys. **67**, 1233 (2004)
2. H.G. LeDuc, L.B. Coleman, Phys. Rev. B **31**, 933 (1985)
3. K. Wakamura, Phys. Rev. B **59**, 3560 (1999)
4. R. Sudharsanan, T.K.K. Srinivasan, S. Radhakrishna, Solid State Ionics **13**, 277 (1984)
5. P. Hermet, M. Goffinet, J. Kreisel, P. Ghosez, Phys. Rev. B **75**, 220102 (2007)
6. S. Hull, D.A. Keen, P. Berastegui, J. Phys.: Condens. Matter **14**, 13579 (2002)
7. I. Bolesta, I. Karbovnyk, O. Futey, S. Velgosh, Rad. Effects and Defects in Solids **158**, 157 (2003)
8. I. Karbovnyk, Ferroelectrics **317**, 15 (2005)
9. S. Bellucci, I. Bolesta, I. Karbovnyk, R. Hrytskiv, G. Fafilek, A.I. Popov, J. Phys.: Cond. Matt. **20**, 474211 (2008)
10. M.C. Guidi, M. Piccinini, A. Marcelli, A. Nucara, P. Calvani, E. Burattini, J. Opt. Soc. Am. A **22**, 2810 (2005)
11. A. Bocci, A. Marcelli, E. Pace, A. Drago, M. Piccinini, M.C. Guidi, A.D. Sio, D. Sali, P. Morini, J. Piotrowski, Nuclear Instruments and Methods in Physics Research A **580**, 190 (2007)
12. C. Balasubramanian, S. Bellucci, G. Cinque, A. Marcelli, M.C. Guidi, M. Piccinini, A. Popov, A. Soldatov, P. Onorato, J. Phys.: Cond. Matt. **18**, S2095 (2006)
13. I. Bolesta, S. Velgosh, Y. Datsiuk, I. Karbovnyk, V. Lesivtsiv, T. Kulay, A.I. Popov, S. Bellucci, M.C. Guidi, A. Marcelli et al., Radiat. Meas. **42**, 851 (2007)
14. S. Bellucci, A.I. Popov, C. Balasubramanian, G. Cinque, A. Marcelli, I. Karbovnyk, V. Savchyn, N. Krutyak, Radiat. Meas. **42**, 708 (2007)
15. A. Voloshynovskii, P. Savchyn, I. Karbovnyk, S. Myagkota, M.C. Guidi, M. Piccinini, A.I. Popov, Solid State Commun., in press (2009)
16. R. Dovesi, V.R. Saunders, C. Roetti, R. Orlando, C.M. Zicovich-Wilson, F. Pascale, B. Civalleri, K. Doll, N.M. Harrison, I.J. Bush et al., *CRYSTAL06 User's Manual*, University of Torino, Torino (2006), http://www.crystal.unito.it/
17. H.J. Monkhorst, J.D. Pack, Phys. Rev. B **13**, 5188 (1976)
18. R.H. Lyddane, R.G. Sachs, E. Teller, Phys. Rev. **59**, 673 (1941)
19. F. Gervais, B. Piriou, Phys. Rev. B **10**, 1642 (1974)
20. R.J. Gonzalez, R. Zallen, H. Berger, Phys. Rev. B **55**, 7014 (1997)
21. J.L. Duarte, J.A. Sanjurjo, R.S. Katiyar, Phys. Rev. B **36**, 3368 (1987)
22. R. Frech, Phys. Rev. B **13**, 2342 (1976)
23. D. De Sousa Meneses, P. Simon, Y. Luspin, Phys. Rev. B **61**, 14382 (2000)
24. D. Stroud, Superlatt. Microstr. **23**, 567 (1998)
25. J.P. Perdew, Y. Wang, Phys. Rev. B **33**, 8800 (1986)
26. J.P. Perdew, Y. Wang, Phys. Rev. B **45**, 13244 (1992)
27. J.P. Perdew, K. Burke, M. Ernzerhof, Phys. Rev. Lett. **77**, 3865 (1996)
28. A.D. Becke, J. Chem. Phys. **98**, 5648 (1993)
29. C.M. Zicovich-Wilson, F. Pascale, C. Roetti, V.R. Saunders, R. Orlando, R. Dovesi, J. Comput. Chem. **25**, 1873 (2004)
30. E. Kroumova, M.I. Aroyo, J.M. Perez-Mato, A. Kirov, C. Capillas, S. Ivantchev, H. Wondratschek, Phase Transitions **76**, 155 (2003)